Complex molecular dynamics of a symmetric model discotic liquid crystal revealed by broadband dielectric, thermal and neutron spectroscopy

Arda Yıldırım[1], Christina Krause[1], Reiner Zorn[2], Wiebke Lohstroh[3], Gerald J. Schneider[4,§], Michaela Zamponi[4], Olaf Holderer[4], Bernhard Frick[5], Andreas Schönhals[1,*]

[1]Bundesanstalt für Materialforschung und -prüfung (BAM), Unter den Eichen 87, 12205 Berlin, Germany

[2]Forschungszentrum Jülich GmbH, Jülich Centre for Neutron Science (JCNS-1) and Institute for Complex Systems (ICS-1), 52425 Jülich, Germany

[3]Heinz Maier-Leibnitz Zentrum (MLZ), Technische Universität München, Lichtenbergstraße 1, 85748 Garching, Germany

[4]Forschungszentrum Jülich GmbH, Jülich Centre for Neutron Science at MLZ, Lichtenbergstr. 1, 85748 Garching, Germany

[5]Institut Laue-Langevin, 71 avenue des Martyrs, 38042 Grenoble Cedex 9, France

§Current address: Department of Chemistry and Department of Physics &Astronomy, Louisiana State University, Baton Rouge, LA 70803, USA.

Abstract:

The molecular dynamics of the triphenylene-based discotic liquid crystal HAT6 is investigated by broadband dielectric spectroscopy, advanced dynamical calorimetry and neutron scattering. Differential scanning calorimetry in combination with X-ray scattering reveals that HAT6 has a plastic crystalline phase at low temperatures, a hexagonally ordered liquid crystalline phase at higher temperatures and undergoes a clearing transition at even higher temperatures. The dielectric spectra show several relaxation processes: a localized γ-relaxation a lower temperature and a so called α_2-relaxation at higher temperatures. The relaxation rates of the α_2-relaxation have a complex temperature dependence and bear similarities to a dynamic glass transition. The relaxation rates estimated by hyper DSC, Fast Scanning calorimetry and AC Chip calorimetry have a different temperature dependence than the dielectric α_2-relaxation and follows the VFT-behavior characteristic for glassy dynamics. Therefore, this process is called α_1-relaxation. Its relaxation rates show a similarity with that of polyethylene. For this reason, the α_1-relaxation is assigned to the dynamic glass transition of the alkyl chains in the intercolumnar space. Moreover, this process is not observed by dielectric spectroscopy which supports its assignment. The α_2-relaxation was assigned to small scale translatorial and/or small angle fluctuations of the cores.

The neutron scattering data reveal two relaxation processes. The process observed at shorter relaxation times is assigned to the methyl group rotation. The second relaxation process at longer time scales agree in the temperature dependence of its relaxation rates with that of the dielectric γ-relaxation.

Introduction

The molecular dynamics related to the glass transition is a current problem of condensed matter physics.[1-6] Till today it is only partly understood why a glass-forming system freezes in a disordered, glassy state instead forming a crystal. One of the most challenging fact is the dramatic increase of both the structural relaxation time τ (relaxation rate $f_p=1/(2\pi\tau)$) and the viscosity when a glass-forming system is cooled down. When decreasing the temperature by a factor of two towards the glass transition temperature T_g, τ increases by more than 14 orders of magnitude and microscopic and macroscopic time scales are bridged. The corresponding molecular process is called α-relaxation (structural relaxation) or dynamic glass transition. In the vicinity of T_g the temperature dependence of τ or $f_p=1/(2\pi\tau)$ can be approximated by the Vogel-Fulcher-Tammannequation[7-9]

$$\log f_p = \log f_\infty - \frac{B}{T-T_0} . \quad (1)$$

Here f_∞ is the relaxation rate at infinite temperatures and B a constant witch is related to the fragility strength $D=B/(\ln(10)\ T_0)$ (D-fragility parameter). The fragility concept to the glass transition is a useful scheme to classify glass-forming systems.[10,11] Glass-forming systems are classified as "fragile" if the temperature dependence of τ deviates strongly from an Arrhenius-type dependence and "strong" if $\tau(T)$ is close to the latter. T_0 is called Vogel or ideal glass transition temperature and empirically found 30 – 70 K below the T_g measured by conventional methods like Differential Scanning Calorimetry (DSC).

In the cooperativity approach to the glass transition,[12-15] which is widely discussed, the strong increase of the relaxation time close to the glass transition temperature is related to the assumption that in an environment of a given molecule other molecules have to re-arrange cooperatively to reach the minimum of a complex energy landscape.

Further dynamical processes are observed, which are relevant for the glass transition besides the α-relaxation. Goldstein and Johari pioneered the idea that a so-called slow β-relaxation can be considered as a precursor of the α-relaxation in cases where the process (true genuine β-relaxation) cannot be assigned to internal degrees of freedom.[16,17] The temperature dependence of the relaxation rate of the β-relaxation is characterized by the Arrhenius law

$$f_p = f_\infty \exp\left(-\frac{E_A}{k_B T}\right) \quad (2)$$

where E_A is the activation energy and k_B the Boltzmann constant.

The most known materials showing a glass transition are the widely studied low molecular weight liquids, silica glasses, or polymers. Besides these materials a glass transition can be also observed for materials with partial order and restricted mobility.[10,11] For the first time, Seki and Suga reported a glass transition of plastic crystals.[18] Further examples for a glass transition in plastic crystal are for instance discussed in references.[19-23] It is worth noting that also discotic liquid crystals show a kind of glassy dynamics as discussed elsewhere.[24-26] Till today it is an open question which molecular processes are responsible for glassy dynamics in systems with restricted mobility and partial order. Investigations on such systems like liquid crystals might be suited to study the glass transition phenomena in general.

Discotic liquid crystals (DLCs) are advanced soft matter materials with a variety of potential application in the field of electronics.[27-29] In principle, discotic liquid crystals are formed by molecules having a disc-like core and longer alkyl chains connected to the core structure. At low temperatures DLCs often form a plastic crystalline phase followed by a hexagonal columnar liquid crystalline phase at higher temperatures where the disc-like molecules are stacked into columns which can be considered as a one-dimensional fluid.[30] Furthermore, the columns are arranged on a hexagonal lattice. The potential applications of DLCs are related to this liquid crystalline hexagonal ordered phase. Besides the hexagonal columnar phase also nematic phases can be observed. At even higher temperature than the range of the hexagonal columnar liquid crystalline phase DLCs undergo an isotropization transition where the molecules become more or less disordered.

In this paper, the molecular dynamics of a triphenylene model system for discotic liquid crystals is investigated by broadband dielectric spectroscopy (BDS), neutron scattering and advanced calorimetric measurements. Recently a study concerning functionalized triphenylene model compounds has been published by some of the authors.[31] It should be noted that in the literature the molecular dynamics of DLCs having a more complex core is reported.[32-33],[34]

Experimental

Materials: The discotic liquid crystal Hexakis(hexa-alkyloxy)triphenylene (HAT6) was purchased from Synthon Chemicals (Bitterfeld, Germany) and used without further purifications. The chemical structure is given in Figure 1. At low temperature HAT6 has a plastic crystal phase, followed by hexagonal ordered columnar liquid crystal phase in the temperature range from 342 K to 372.3 K. At temperatures above 372.3 K, HAT6 is in the isotropic state. All phase transition temperatures were taken from the second heating run of a

differential scanning calorimetry measurement (heating rate 10 K/min, see Figure 1). For experimental details including X-ray scattering data see ref.[35]

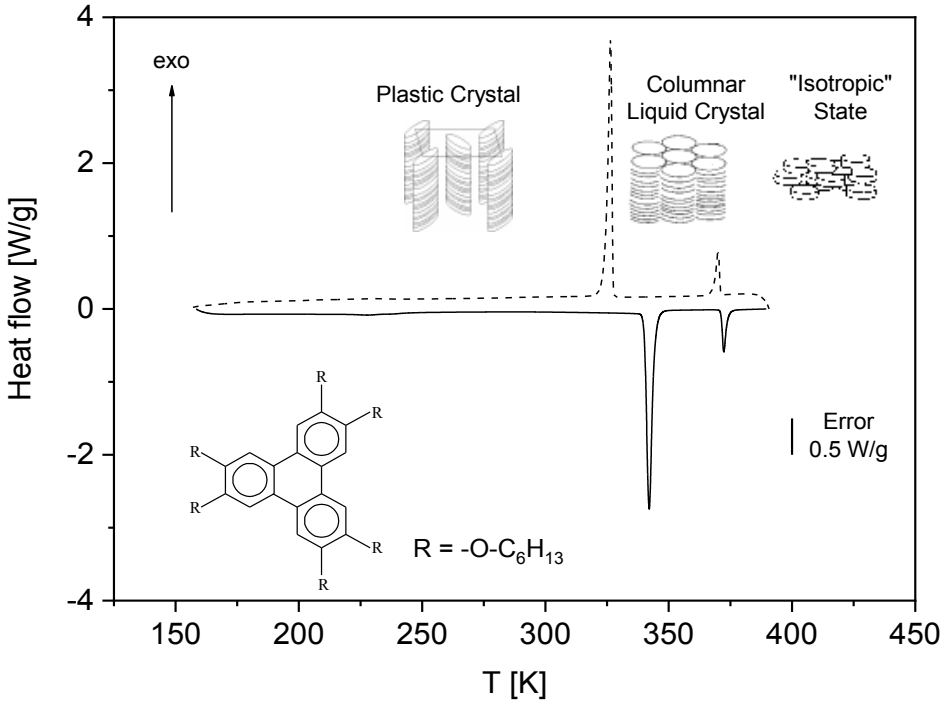

Figure 1: DSC thermogram of HAT6 during cooling (dashed line) and heating (solid line) at a rate of 10 K/min. The inset gives the chemical structure of HAT6. Further the different phases are illustrated.

Differential Scanning Calorimetry (DSC): DSC measurements were carried out by a Perkin Elmer DSC 8500. Nitrogen was used as a purge gas at a flow rate of 20 ml/min for temperatures higher than 173 K. For measurements at lower temperatures than 173 K helium was applied as purge gas also at a flow rate of 20 ml/min. Moreover, the calibration of the DSC was checked before the measurement by measuring an indium standard. A baseline measurement was conducted by measuring an empty pan under the same conditions as the sample.

To investigate the phase transition behavior ca. 6 mg HAT6 was inserted in a standard DSC pan with a volume of 50 µl and investigated in the temperature range from 173 K to 423 K with a heating/cooling rate of 10 K/min. The data were taken from the second heating run.

To investigate the glass transition behavior Hyper DSC with heating rates up to 300 K/min was employed also by utilizing DSC 8500. For these measurements specialized DSC pans are applied allowing for high rates (Perkin Elmer N520-3115, Folding Hyper DSC Aluminum sample pans). In the case of Hyper DSC measurements samples of about 1 mg are used. To

guarantee the same sample state before each heating run the sample was heated to 423 K in the isotropic state and cooled down with a cooling rate of 10 K/min to 173 K.

Fast Scanning Calorimetry (FSC): FSC employing a Mettler-Toledo Flash DSC1, which is a chip-based power compensated DSC, was further used to investigate the glass transition of the samples.[36] The MultiSTAR UFS 1 used in Flash DSC 1 is a twin chip sensors.[37] Because of the chip-based technology heating rates from 10 K/s to 10000 K/s can be applied. As purge gas Nitrogen was used at a flow rate of 40 ml/min. For temperature control a Huber TC100 intercooler was used. The calibration of the Flash DSC 1 was carried out according to the recommendations of the producer. A detailed description can be found in reference 38. The error in the estimated glass transition temperatures results mainly from the thermal lag which is estimated to be ± 3 K.

AC Chip Calorimetry: For AC chip calorimetry the calorimeter chip XEN 39390 (Xensor integrations, Nl) was employed as measuring cell. Two 4-wire heaters (bias and guard heater) are located in the center of a free-standing thin silicon nitride membrane (thickness 1 μm) supported by a Si frame. The nanocalorimeter chip has a theoretical heated hot spot area of about 30×30 μm^2, with an integrated 6-couple thermopile.[39] In addition to the 30×30 μm^2 hot spot also the heater strips contribute to the heated area. A SiO_2 layer with a of thickness 0.5-1 μm) protects the heaters and thermopiles. The sample is melted directly on the sensor at the heated area under a microscope.

A differential approach was used which minimizes the contribution of the heat capacity of the empty sensor to the measured data.[40] In the approximation of thin films (submicron) the heat capacity of the sample C_S is given by

$$C_s = i\omega C_{eff}(\Delta U - \Delta U_0)/P_0 S \qquad (3)$$

where S is the sensitivity of the thermopile, P_0 is the applied heating power. $C_{eff} \equiv C_0 + G/i\omega$ describes the effective heat capacity of the empty sensor were G/iω is the heat loss through the surrounding atmosphere and ω is angular frequency (ω=2πf, f-frequency). $i = \sqrt{-1}$ denotes the imaginary unit. ΔU is the complex differential thermopile voltage for an empty and a sensor with a sample, and ΔU_0 is the complex differential signal obtained for two empty sensors. For identical sensors, ΔU_0=0 holds. For details see reference 40. Absolute values of the complex specific heat capacity[41] can be deduced from the complex differential voltage using calibration techniques. Here the real part of the complex differential voltage and the phase angle are considered.

The temperature-scan-mode was employed, which means that the frequency was kept constant while the temperature was scanned with a heating/cooling rate of 1 K/min … 2.0 K/min depending on the used frequency. The heating power for the modulation was kept constant at about 25 µW, which ensures that the amplitude of the temperature modulation is less than 0.5 K. The frequency is varied between 1 Hz and 1000 Hz

Broadband Dielectric Spectroscopy: The complex dielectric function $\varepsilon^*(f)=\varepsilon'(f) - i\varepsilon''(f)$ is measured in the frequency range from 10^{-2} Hz to $3*10^9$ Hz where ε' and ε'' denote the real and loss part of the complex dielectric function. All measurements were carried out in parallel plate geometry with gold plated brass electrodes. Fused silica spacers were employed to maintain a sample thickness of 50 µm.

In the frequency range from 10^{-2} Hz to 10^7 Hz the measurements were performed by a high-resolution Alpha analyzer with an active sample head (Novocontrol, Montabaur, Germany). For more details see ref.[42]. The diameter of the sample for these measurements was 20 mm.

In the frequency range from 10^6 Hz to $3*10^9$ Hz the measurements were carried out by a coaxial line reflectometer based on the Agilent impedance analyzer E4991. For these measurements, the sample is modelled as part of the inner conductor. For more details see ref.[42] Here the diameter of the sample capacitor was 6 mm.

In both setups, the temperature of the sample was controlled by a Quatro temperature controller (Novocontrol). The temperature stability was better than 0.1 K.

***Broadband Neutron Spectroscopy*:** To cover also a broad time window by inelastic neutron scattering different spectrometer based on different principles are combined. Inelastic neutron scattering is sensitive to molecular motions at microscopic length and time scales.[43] During the scattering process momentum and energy are exchanged between the neutrons and the nuclei of the sample. This yields to information about the space and time dependence of the underlying dynamical processes. The double differential cross section

$$\frac{d^2\sigma}{d\Omega\, d\omega} = \frac{1}{4\pi}\frac{k_f}{k_i}\left(\sigma_{coh}S_{coh}(q,\omega) + \sigma_{inc}S_{inc}(q,\omega)\right) \quad (4)$$

is obtained during a neutron scattering experiment as main experimental quantity. Here q denotes the scattering vector while k_i and k_f are the incident and final wave vectors of the neutron beam respectively. The angular frequency ω is a related to the measured energy transfer ΔE by $\omega=\Delta E/\hbar$. Ω is the solid angle of detection. $S_i(q,\omega)$ are the incoherent and coherent dynamic structure factors (scattering functions), σ_{coh} and σ_{inc} are the scattering cross-sections for coherent and incoherent scattering. HAT6 consists of hydrogen (H), carbon (C),

and oxygen (O). The corresponding scattering cross-sections for coherent and incoherent scattering are given in Table 1. Hydrogen is the strongest incoherent scatterer and the coherent contributions of all nuclei for HAT6 are much smaller. Therefore, the observed scattering is predominantly incoherent and related to the H-distribution in the alkyl chains.

Table 1: Cross-section for incoherent and coherent scattering of the relevant nuclei.

Nuclei	σ_{inc} [barn]	σ_{coh} [barn]
H	80.27	1.756
C	0	5.551
O	0	4.232

Elastic scans: To have an overview about the molecular dynamics at a time scale of ca. 1.7 ns elastic fixed window scans ($\Delta E \approx 0$) are carried out by neutron backscattering employing the backscattering instrument IN16B operated at the Institut Laue-Langevin (ILL, Grenoble, France)[44]. IN16B is a third-generation cold neutron backscattering spectrometer with focusing optics and a rotating phase-space-transform chopper. IN16B was used in standard configuration (unpolished Si-111) with wavelength of the incident neutron beam of 6.271 Å corresponding to a resolution of 0.75 μeV (full width at half maximum). In this configuration the scattering vector q ranges from 0.1 Å to 1.8 Å. From the elastic scattered intensities an effective mean-square displacement $\langle u^2 \rangle_{eff}$ is calculated by a fractal model[45] which in case of a clear separation of elastic and inelastic scattering reduces to the usual Gaussian form

$$I_{el} / I_0 = e^{(-q^2 \langle u^2 \rangle_{eff}/3)} \quad (5)$$

(I_{el} and I_0 are the elastically and totally scattered intensities) but is more reliable in the high $\langle u^2 \rangle_{eff}$ value region. I_0 was measured at temperatures below 2K with an increased statistic. The measurements were carried out with a heating rate of 1.9 K/min below 300 K and 0.43 K/min in the range 300–470 K where the more interesting dynamics is observed. These rates correspond to one data point per 4 K and per 1 K, respectively.

Combination of neutron time-of-flight and backscattering: To cover a broad time range by neutron scattering too, neutron time-of-flight was combined with neutron backscattering. Time-of-flight scattering was carried out at the multi-chopper cold neutron time-of-flight spectrometer TOFTOF.[46] It is operated by the Technische Universität München at the Heinz

Maier-Leibnitz Zentrum (MLZ) in Garching, Germany. An incident wavelength of λ_n= 5.0 Å was used employing a standard configuration of TOFTOF. This corresponds to a resolution of 85–100 μeV (full width at half maximum) and a maximal accessible elastic scattering vector of q=2.3 $Å^{-1}$. Figure 2a depicts the incoherent dynamic structure factor for HAT6 measured at TOFTOF for different temperatures. In comparison to the resolution measured at 4 K (see below) the spectra measured for higher temperatures show the characteristic quasielastic broadening.

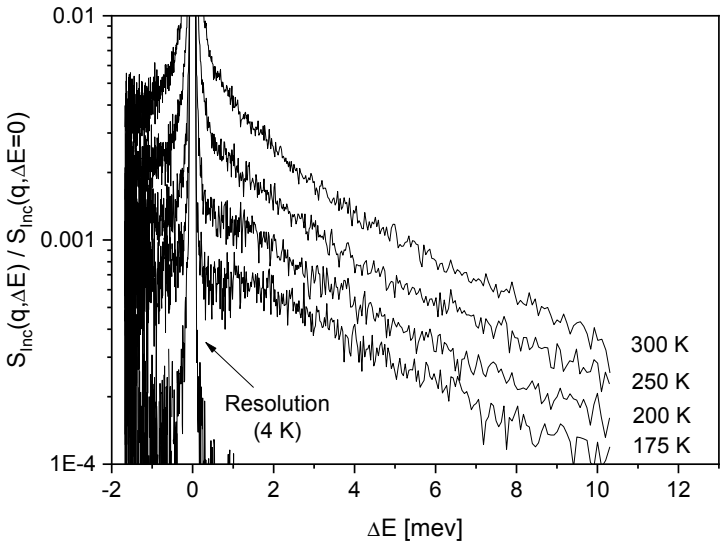

Figure 2a: Neutron Time-of-Flight spectra measured at TOFTOF for the indicated temperatures at a q vector of 1.42 $Å^{-1}$. The spectra were normalized by the peak value of the elastic line. The scattering of the empty can is already subtracted. The statistics of the measurement can be judged from the scatter of the data.

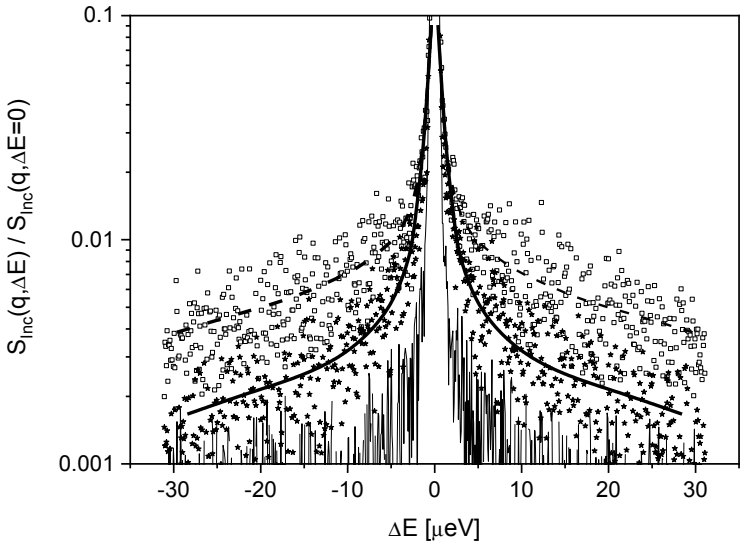

Figure 2b: Neutron backscattering spectra from SPHERES at an angle of 90°. The spectra were normalized by the peak value of the elastic line. The scattering of the empty can is already subtracted. Thin solid line – 4 K (resolution), asterisk – 200 K, squares – 300 K. The thick solid line is a guide to the eyes for the data at 200 K where the dashed line is a guide to the eyes for the data at 300 K. The statistics of the measurement can be judged from the scatter of the data.

Neutron backscattering spectra were taken at the high-resolution spectrometer SPHERES.[47,48] SPHERES is a third-generation cold neutron backscattering spectrometer with focusing optics and a rotating phase-space-transform chopper. It is operated by the Jülich Centre for Neutron Science JCNS, Forschungszentrum Jülich at the MLZ. SPHERES was used in standard configuration with an incident wavelength of λ_n= 6.27 Å and a maximal resolution of 0.64 μeV. The maximal accessible elastic scattering vector was q=1.76 Å^{-1}. Figure 2b gives the incoherent dynamic structure factor for HAT6 measured at SPHERES for different temperatures. Also, here the quasielastic broadening of the spectra with respect to the resolution is observed.

To obtain the resolution for both instruments R(q,ΔE) the sample was measured at 4 K. At this temperature, it can be expected that except for quantum-mechanical zero-point motions all molecular fluctuations leading to quasielastic scattering are frozen. Data from TOFTOF were evaluated by the program INX[49] featuring TOF to energy conversion, background subtraction, vanadium normalization, and self-attenuation correction. Data from SPHERES were evaluated by the program SQW[50] which applies backscattering normalization, vanadium normalization, self-attenuation correction, and in addition performs an attenuation correction

on the background to be subtracted. Both programs produce an effective (scattering cross section weighted) S(q,ΔE).

Because of the large difference in the resolution of TOFTOF and SPHERES (see Figure 2) the dynamic structure factors $S_{Inc}(q,\Delta E)$ were Fourier transformed and divided by the Fourier transform of the corresponding resolution. This procedure leads to absolute values of the incoherent intermediated scattering function $S_{Inc}(q,t)$ which can be jointly analyzed for data measured on both instruments in time domain. The $S_{inc}(q,t)$ data sets from time-of-flight and backscattering spectroscopy were corrected for multiple scattering using a procedure acting in time domain[51]. Because the exact scattering geometry cannot be determined, the multiple scattering fraction was fitted to optimize the limit $S_{inc}(q\rightarrow 0,t)=1$. The resulting multiple scattering fractions were 15% and 20% with respect to the first scattering for SPHERES and TOFTOF respectively.

Results

Broadband dielectric spectroscopy: Figure 3 gives the dielectric loss spectra of HAT versus frequency and temperature in a 3D representation. Several dielectrically active processes are observed. At lowest temperature a so called γ-relaxation is observed indicated by a peak. At higher temperatures than the γ-relaxation a so-called α_2-relaxation becomes active. At even higher temperatures a conductivity contribution is observed.

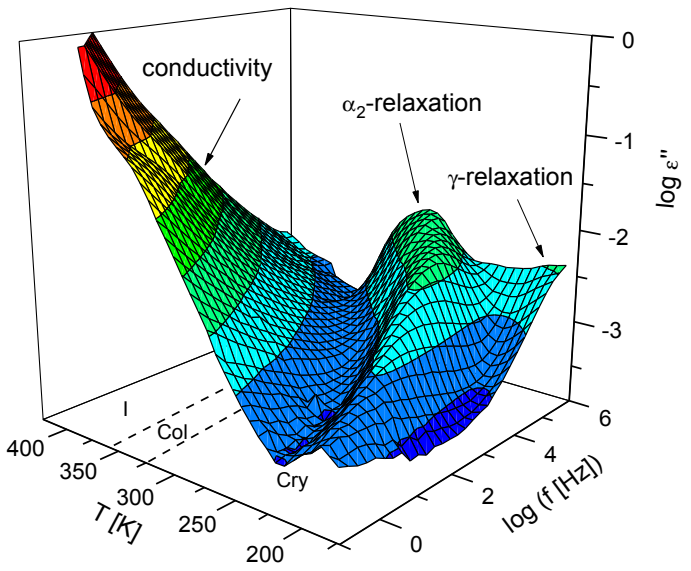

Figure 3: Dielectric loss versus frequency and temperature for HAT6 in a 3D representation

during cooling in the frequency range from 10^{-1} Hz to 10^{6} Hz. I – isotropic, Col – columnar hexagonal ordered, and Cry – plastic crystalline phase.

In order to analyze the dielectric data quantitatively the model function of Havriliak and Negami (HN-function) was fitted to the data. The HN-function reads

$$\varepsilon^*_{HN}(\omega) = \varepsilon_\infty + \frac{\Delta\varepsilon}{\left(1+(i\omega\tau_{HN})^\beta\right)^\gamma} \quad (6)$$

where $\Delta\varepsilon$ denotes the dielectric strength. The fractional parameters β and γ ($0<\beta$; $\beta\gamma\leq 1$) describe the symmetric and the asymmetric broadening of the complex dielectric function with respect to the Debye one.[52] The frequency of the maximum in the dielectric loss f_p (relaxation rate) is related to the relaxation time τ_{HN} and is given by

$$f_p = \frac{\omega}{2\pi} = \frac{1}{2\pi\tau_{HN}} \sin\left(\frac{\pi\beta}{2+2\gamma}\right)^{1/\beta} \sin\left(\frac{\pi\beta\gamma}{2+2\gamma}\right)^{-1/\beta}. \quad (7)$$

This analysis results in the relaxation rate f_p and the dielectric strength $\Delta\varepsilon$ for the different relaxation processes. Conduction effects are treated by adding the contribution $\varepsilon''_{cond} = {\sigma_0}/{(\omega^s\ \varepsilon_0)}$ to the dielectric loss. σ_0 is related to the DC conductivity of the sample and ε_0 is the permittivity of vacuum. The parameter s ($0<s\leq 1$) describes for s=1 Ohmic and for s<1 non-Ohmic effects in the conductivity. Details can be found in reference.[52] Figure 4 gives some examples for the fitting procedure in the temperature range of the α_2-relaxation.

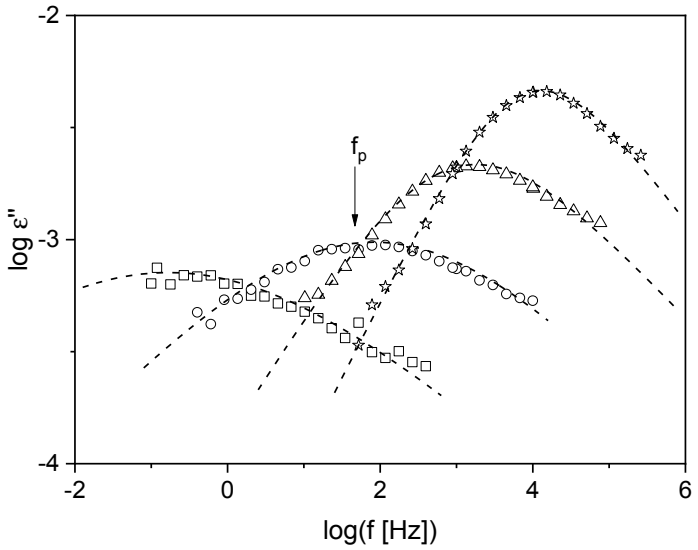

Figure 4: Dielectric loss versus frequency for different temperatures: square – 183 K, circle – 204 K, triangle – 219 K, and asterisk – 234 K. In the frequency range from 1 Hz to 10^5 Hz the error of the data corresponds approximately to the size of the symbols. Dashed lines are fits of the HN-function to the data.

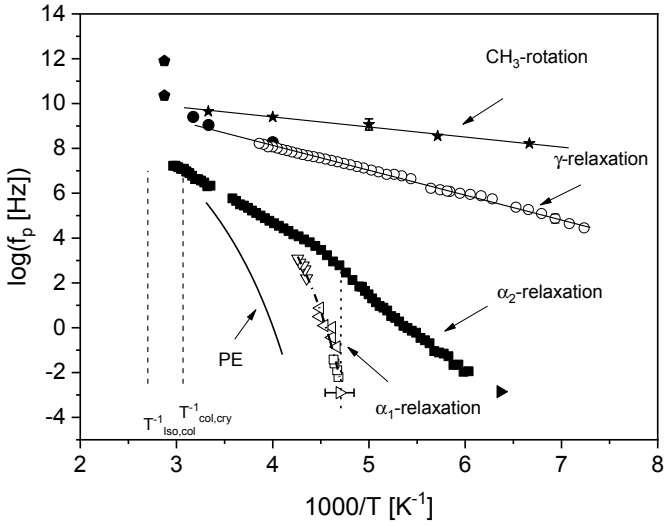

Figure 5: Relaxation map of HAT6: Asterisk – methyl group rotation, Open circles – dielectric γ-relaxation. The solid lines are corresponding fits of the Arrhenius equation to the data. Solid squares – dielectric α_2-relaxation, Solid right oriented triangle – low temperature glass transition estimated from DSC experiments with He as purge gas. Thermal data: Right oriented open triangle – DSC experiment with 10 K/min, open squares – Hyper DSC experiments, left oriented open triangles – Flash DSC experiments, down sited open triangles – AC chip calorimetry. The dashed-dotted line is a fit of the VFT – equation to the data. Solid curved line – dielectric α-relaxation rates for polyethylene taken from reference 57, solid pentagons – neutron scattering data taken from reference 60. Typical error bars are given for thermal and neutron data. The error bars of the dielectric data are smaller than the

size of the symbols.

Figure 5 gives the relaxation rate versus inverse temperature in the Arrhenius diagram. The data for the γ-relaxation follow the Arrhenius law, with an activation energy of 20.6 ± 2 kJ/mol. In reference[53] a quite similar value of 23 kJ/mol is reported. Moreover, the data for the γ-relaxation of HAT6 show a close resemblance to the temperature dependence of the relaxation rates of the γ-relaxation found for polyethylene as also discussed in reference.[53] Therefore it is concluded that the γ-relaxation of HAT6 is related to localized fluctuations of methylene groups.

In comparison to the temperature dependence of the γ-relaxation that of the α_2-relaxation is more complex (see Figure 5). At first glance the temperature dependence of the relaxation rates of the α-relaxation follows neither the Arrhenius nor the VFT equation. It seems that the temperature dependence of log $f_{p,\alpha 2}(T)$ changes around 230 K.

Differential scanning calorimetry: To investigate the glass transition behavior of HAT6 Hyper DSC[54] with heating rates up to 300 K/min was carried out. Before each heating run the sample was cooled down from the isotropic state (333 K) to the plastic crystalline phase with the same cooling rate of 10 K/min. Figure 6 depicts the heat flow versus temperature for selected heating rates. A step-like change in the heat flow is detected indicating a glass transition. With increasing heating rate, the step becomes more pronounced because the measured heat flow is proportional to the heating rate and shifts to higher temperatures. T_g was estimated from the half-step height of the step. For comparison with the dielectric results a thermal relaxation rate is calculated by[55,56]

$$f_p = \frac{\dot{T}}{2\,\pi\,a\,\Delta T_g}, \qquad (8)$$

where $\dot{T}$ is the heating rate and ΔT_g is the width of the glass transition estimated as the difference between the endset and the onset temperatures of the step of the glass transition. (a is a constant in the order of one.) The observed overshoot in the heat flow might result in a larger error in ΔT_g. The thermal relaxation rates estimated by Hyper DSC was included in the relaxation map of HAT6 (see Figure 5).

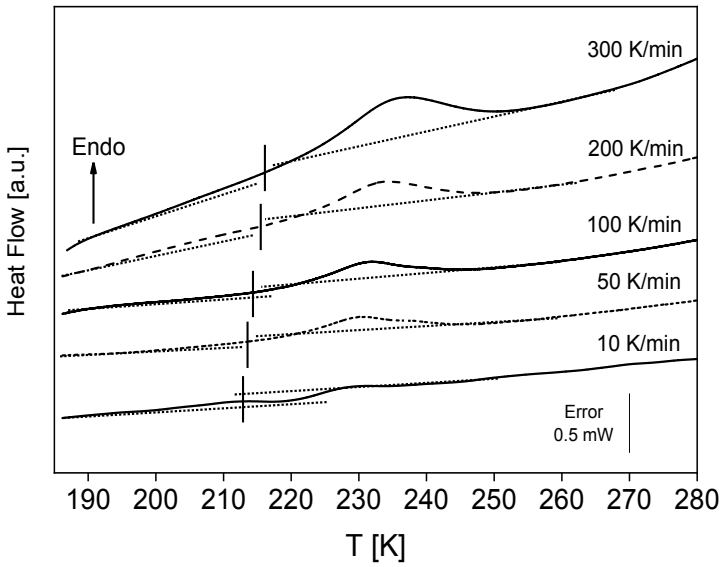

Figure 6: DSC thermograms measured by HyperDSC at the indicated heating rates. The curves are shifted along the y-scale for sake of clarity.

In addition to Hyper DSC, fast scanning calorimetry[36] employing a Flash DSC 1 was further used to investigate the glass transition of HAT6. Heating rates from 10 K/s to 500 K/s were used. Also, here prior each heating run the sample is cooled down from 333 K to the plastic crystalline state (183 K) with same cooling rate of 500 K/s. Figure 7 gives typical heat flow curves at the indicated heating rates. The glass transition is observed and a T_g is estimated. The heating rates are converted into a thermal relaxation rate according to Equ. 8 and included to Figure 5.

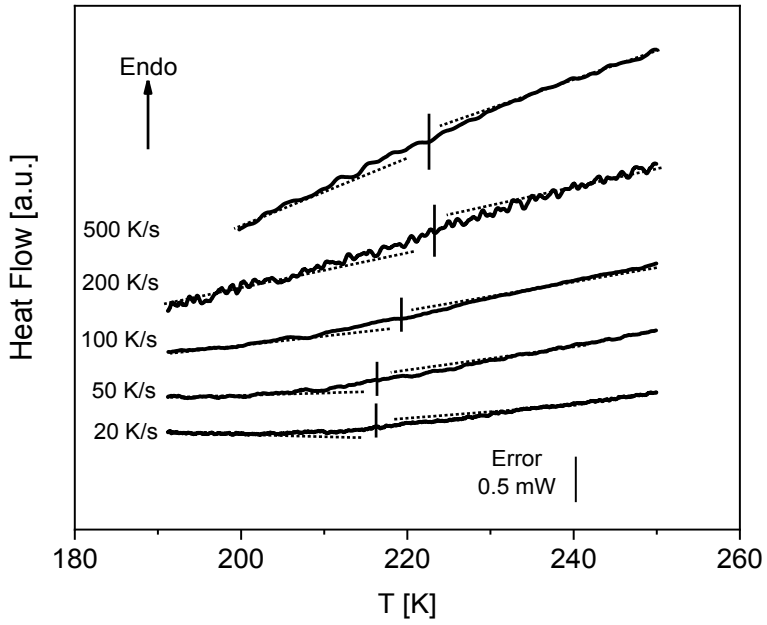

Figure 7: DSC thermograms measured by Flash DSC at the indicated heating rates. The curves are shifted along the y-scale for sake of clarity.

Figure 8 gives the real part of the complex differential voltage U_R measured with AC chip calorimetry as a measure for the heat capacity. A step-like change of U_R is observed with increasing temperature indicating the dynamic glass transition. A dynamic glass transition temperature $T_g^{dynamic}$ is estimated from the mid-step height of ΔU_R and added together with the measuring frequency to the relaxation map of HAT6 (Figure 5).

It becomes obvious from Figure 5 that the thermal data, which can be approximated in the measured frequency range by the VFT equation, do not agree with the dielectric results. The thermal data are shifted to higher temperatures in comparison to the dielectric ones and have also a different temperature dependence. Therefore, this relaxation process is called α_1-relaxation. Further the change observed in the temperature dependence of the dielectric α_2-relaxation seems to correspond to the thermal glass transition temperature of HAT6 measured at a relaxation rate of ca. 10^{-2} Hz.

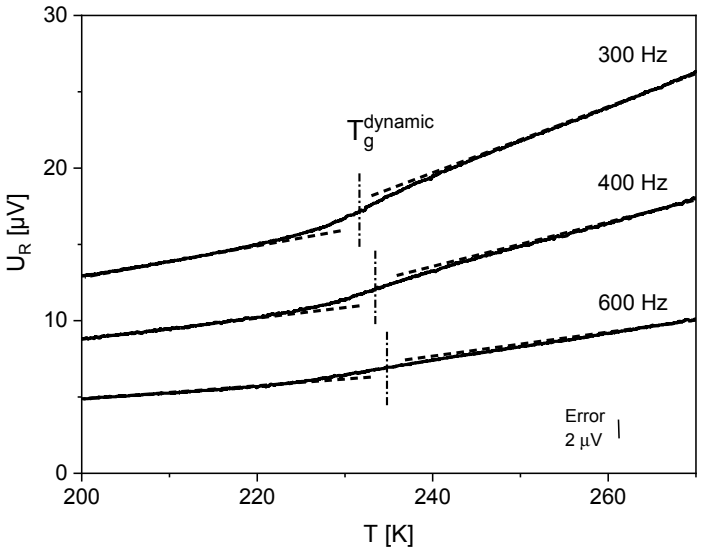

Figure 8: Temperature dependence of the real part U_R of the complex differential voltage measured at the indicated frequencies.

The temperature dependence of the calorimetric relaxation rates (α_1-relaxation) shows a close resemblance with that of dielectric α-process of polyethylene.[57] From this coincidence, discussed also for other discotic liquid crystals[24,25,31,58] and materials like ionic liquid crystals too[59], the α_1-relaxation is assigned to cooperative fluctuations (glassy dynamics) of the alkyl chains in the intercolumnar space. This glass transition can be considered as a glass transition in a three-dimensional confinement. Because no dipole moment is involved in these fluctuations this process is not observed by dielectric spectroscopy, in contrast to functionalized triphenylene compounds.[31] This result confirms further the molecular assignment of the α_1-relaxation.

To investigate the molecular origin of the α_2-relaxation DSC measurements under He atmosphere are carried out (see figure 9). Measurements with He as purge gas allows for lower measurements temperature than these carried out with nitrogen. The corresponding DSC thermogram shows two glass transitions: one at higher temperatures around 213 K which is already discussed above. A second step-like change of the heat flow is observed at lower temperatures around 157 K. This data point is included in figure 5. It agrees well with the dielectric α_2-relaxation. From that coincidence it is concluded that the α_2-relaxation corresponds to a glass transition.

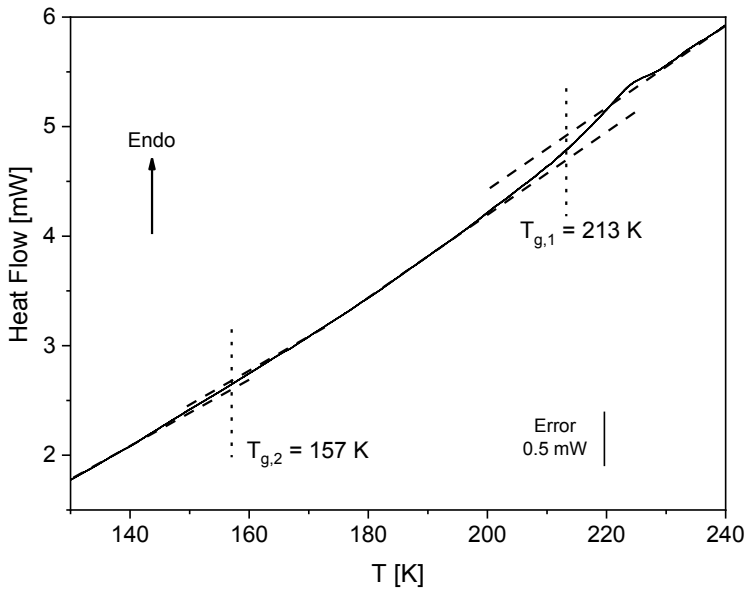

Figure 9: Heat flow versus temperature for a DSC experiment during heating carried out under He atmosphere. The heating rate was 10 K/min.

As discussed in ref. 31, because $T_{g,2}$ is much lower than $T_{g,1}$ this means that the cooperative fluctuations of the alkyl chains are frozen. The only motional processes which seems possible are small scale fluctuations of the cores. Indeed, molecular dynamics simulations predict translational movements of the core (parallel and perpendicular to the column axis), where alkyl chains motions only weakly correlate with the parallel translation of the core.[60] Therefore, the α_2-relaxation is assigned to small scale translational and/or small angle rotational fluctuations of the cores. These fluctuations take probably place in the distorted regions of the columns. The oxygen atoms which can create the only possible dipole moment in the system are located close to the cores. Therefore, this process can be detected by dielectric spectroscopy. As discussed above the columns can be considered as a one-dimensional liquid. For this reason, the α_2-relaxation can be also assigned to glassy dynamics in a one-dimensional liquid.

In the framework of the fluctuation approach[61] to the glass transition a length scale ξ for the cooperative fluctuations can be derived

$$\xi \approx \sqrt[3]{\frac{k_B T_g^2 \Delta\left(\frac{1}{c_P}\right)}{\rho(\delta T)^2}} \qquad (9)$$

where $\Delta(1/c_p)=1/c_{p,glass}-1/c_{p,liquid}$ were $c_v \approx c_P$ is assumed. ρ is the density and δT is the width of the glass transition. The most important quantity influencing the value of the cooperativity length scale is the width of the glass transition. For conventional polymers δT is found to be ca. 10 to 20 K for comparable heating rates. Figure 9 shows that the width of the glass transition for α_2-

relaxation is extremely broad. In turn this means that the cooperativity length scale for the α_2-relaxation is expected to be quite small. This expected small value of the cooperativity length scale of the α_2-relaxation is in agreement with the assigned molecular mechanism. Unfortunately, no quantitative values could be deduced here due to the large uncertainties in the estimation of δT.

The Debye theory of dielectric relaxation predicts for the temperature dependence of the dielectric strength $\Delta\varepsilon$[55,56,62]

$$\Delta\varepsilon = \frac{1}{3\varepsilon_0}\frac{\mu^2}{k_B T}\frac{N}{V} \qquad (10)$$

where μ^2 is the mean squared dipole moment and N/V is the number density of involved dipoles. For glassy dynamics it is known that $\Delta\varepsilon$ decreases with increasing temperature.[63] Already from the raw data given in Figure 3 and 4 it becomes obvious the $\Delta\varepsilon_2$ for the α_2-relaxation has a more complex temperature dependence which seems to increase with increasing temperature. In figure 10 the dielectric strength for the α_2-relaxation is plotted versus temperature. $\Delta\varepsilon_2$ increases slightly with increasing temperature for low temperatures. At around 208 K this temperature dependence changes to a much stronger dependence. The temperature of 208 K corresponds to the glass transition temperature T_{g1}=213 K. At T_{g1} the alkyl chain in the intercolumnar space become mobile. This means the intercolumnar space becomes more and more soft with further increase of temperature. For that reason, constraints to the fluctuations of the core superimposed from the frozen alkyl chain will be more and more released. This will ease the fluctuation of the cores leading to an increase of the number density of the related dipoles or to an increase of its fluctuation angle which would likewise lead to an increase of $\Delta\varepsilon_2$. The observed temperature dependence of $\Delta\varepsilon_2$ of the α_2-relaxation supports its molecular assignment. Moreover, the change in the temperature of $\Delta\varepsilon_2$ corresponds to the change in the temperature dependence of the relaxation rate of the α_2-relaxation. A similar behavior was also observed for different nanoconfined soft matter systems.[64-68]

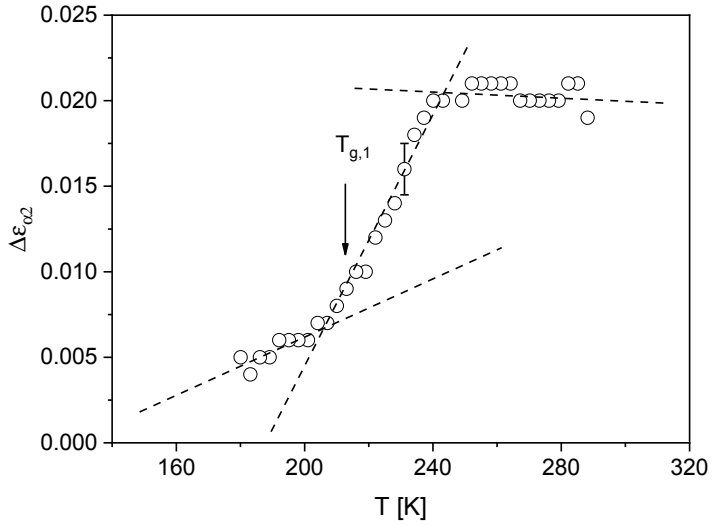

Figure 10: Dielectric strength of the α_2-relaxation $\Delta\varepsilon_2$ versus temperature. An example of a typical error bar for the data is given.

At temperatures above 240 K $\Delta\varepsilon_2$ starts to decrease as expected for glassy dynamics.

Neutron scattering: Figure 11 gives the temperature dependence of the mean squared displacement $\langle u^2 \rangle_{eff}$. At low temperatures the data measured at IN16B shown here agree with preliminary results obtained from experiments carried out on IN10 (data not shown here).[69] At higher temperature both data sets give slightly different values for $\langle u^2 \rangle_{eff}$ due to the different analysis method. As a first result, the phase transitions of HAT6 are also detected by changes in the temperature dependence of $\langle u^2 \rangle_{eff}$ where the estimated values agree with the phase transition temperatures obtained by DSC.

The inset of figure 11 gives $\langle u^2 \rangle_{eff}(T)$ up to 300 K. Several processes can be detected by changes of the temperature dependence of $\langle u^2 \rangle_{eff}$. At lowest temperatures the mean squared displacement is due to vibrations as discussed in references.[35,70] A step-like change of $\langle u^2 \rangle_{eff}(T)$ is observed in the temperature range from approximately 100 K to 150 K. From the literature it is known that at these temperatures the methyl group rotations become active at a time scale of ca. 1 ns.[71,72] The chemical structure of HAT6 (see Figure 1) shows that there are 6 methyl groups per molecule. Therefore, the molecular process taking place between 100 K and 150 K is assigned to the methyl group rotation in HAT6. This will be further discussed in detail below.

In the temperature range from 150 K to ca. 220 K a further change of $\langle u^2 \rangle_{eff}(T)$ is detected which is related to the γ-relaxation evidenced also be dielectric spectroscopy.

At around 220 K, another change in the temperature dependence of the mean squared displacement is observed. This change in the temperature dependence of $\langle u^2 \rangle_{eff}(T)$ coincides well in its temperature position with the glass transition (α_1-relaxation) observed by DSC (see Figure 6). Therefore, this change in the temperature dependence of the mean squared displacement is assigned to the glass transition.

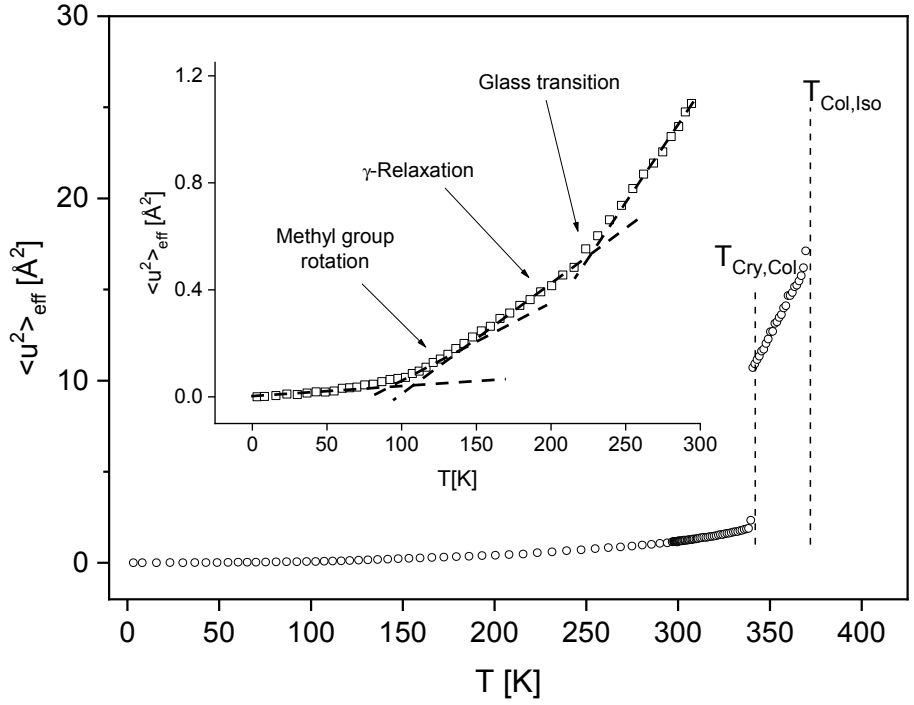

Figure 11: Temperature dependence of the effective mean squared displacement $\langle u^2 \rangle_{eff}$. The inset shows $\langle u^2 \rangle_{eff}(T)$ up to 300 K.

To investigate the molecular mobility observed by the temperature dependence of the mean squared displacement in more detail, quasielastic neutron scattering is carried out. The inset of Figure 12 depicts the incoherent intermediate time dependent scattering function $S_{Inc}(q,t)$ at 200 K at q-vector of q=1.8 Å^{-1}. The data in the range from 0.1 ps to 30 ps corresponds to measurements on TOFTOF while the data from 30 ps to ca. 3 ns were measured at SPHERES. A single decay of $S_{Inc}(q,t)$ is observed at that temperature which is assigned to the methyl group rotation. The methyl group rotation is usually described in terms of the Rotation Rate Distribution Model (RRDM).[71] For simplicity here the data are analyzed by fitting a stretched exponential to $S_{Inc}(q,t)$

$$S_{Inc}(q,t) = DWF * \left((1 - EISF_M) \exp\left(-\left(\frac{t}{\tau_M} \right)^{\beta_M} \right) + EISF_M \right). \quad (11)$$

Here DWF symbolizes the Debye-Waller factor, $EISF_M$ is the Elastic Incoherent Structure Factor for methyl group rotation. τ_M is the relaxation time for methyl group rotation and β_M the corresponding stretched exponential parameter. As expected for a localized process the relaxation time τ_M is independent of the q vector (not shown here).

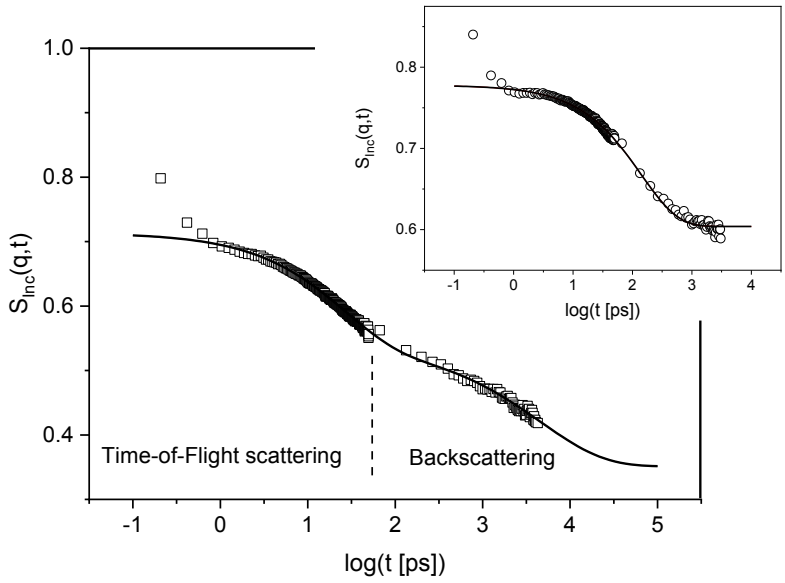

Figure 12. Incoherent intermediate time dependent scattering function $S_{Inc}(q,t)$ versus time at T=250 K for q=1.8 $Å^{-1}$. The inset depicts $S_{Inc}(q,t)$ versus time for T=200 K for q=1.8 $Å^{-1}$.

The most straightforward model for the Elastic Incoherent Structure Factor of the methyl groups $EISF_M$ is that of jump rotation in a threefold potential $V(\phi)\sim(1-\cos(3\phi))/2$ which results from the three equivalent energy minima with respect to the rotation angle Φ of the methyl group. One obtains for the $EISF_M$[71,73]

$$EISF_M(q) = \frac{1}{3}\left(1 + 2\frac{\sin(\sqrt{3}\,qr)}{\sqrt{3}\,qr}\right) \qquad (12)$$

where r = 1.027 Å is the radius of the circle spanned by the positions of the hydrogen nuclei of the methyl group. Figure 13 depicts the $EISF_M$ as calculated from Eq. 12 in comparison to the experimental data obtained at T=150 K. The experimental data deviate significantly from the calculated value. A much higher contribution of elastic scattering is observed than predicted by Eq. 12. The derivation of Eq. 12 assumes that all hydrogen nuclei in the system are located in methyl groups and participate in the methyl group rotation. The chemical

structure of HAT6 (see Figure 1) shows that most hydrogens are located in the alkyl chains in CH_2. At the temperatures were the methyl group rotation is active the methylene groups are immobilized. Therefore, it can be assumed that the hydrogens of the CH_2 scatter elastically. Therefore, Eq. 12 has to be corrected for that elastic scattering as already discussed in references[51,7274]

$$\mathrm{EISF_{M,corr}(q)} = (1 - \mathrm{C_{fix}})\mathrm{EISF_M(q)} + \mathrm{C_{fix}} \quad (13)$$

where C_{fix} is the fraction of hydrogen nuclei which are immobilized at the time scale of the methyl group rotation. Figure 13 shows that Eq. 13 describes the experimental data well. For C_{fix} a value of C_{fix} of 0.736 is obtained. The structure of HAT6 contains 84 hydrogen nuclei where 18 hydrogen nuclei are located in the methyl groups. From that numbers one can calculated the fraction of immobilized hydrogen nuclei to (84-18)/84=0.785. This theoretical number corresponds well to the value of 0.736 extracted from the fit.

From the relaxation time τ a mean relaxation time is calculated by

$$< \tau_{av} > = \frac{\tau}{\beta}\,\Gamma(\beta^{-1}) \quad (14)$$

where $\Gamma(x)$ is the Gamma function. The estimated relaxation rate for the methyl group rotation is included in Figure 5. As expected, the temperature dependence of the relaxation rate of the methyl group rotation follows the Arrhenius equation with an activation energy of 12 ± 2 kJ/mol. This value is typical for the CH_3 rotation for instance also for polymers.[71]

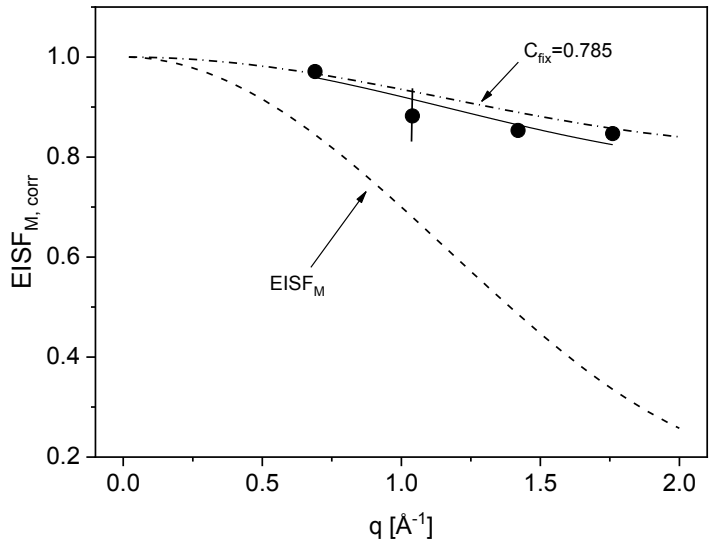

Figure 13. EISF versus q: circles – $EISF_M$ at T=150 K. Solid line – fit of Equ. 13 to the data. Dashed line – calculated according to Equ. 12. Dashed -dotted line – calculated according to Equ. 13 with C_{fix}=0.785 (theoretical value). A typical error bars is given.

For temperatures higher than 200 K the incoherent intermediate time dependent scattering function $S_{Inc}(q,t)$ shows a two-step decay indicating two relaxation processes (see Figure 12). It is interesting to note that even for the highest temperature, $S_{Inc}(q,t)$ does not decay to zero. This means that there is a second EISF related to the spatial signature of the second relaxation process.

$S_{Inc}(q,t)$ for temperature higher than 200 K is analyzed by two stretched exponentials

$$S_{Inc}(q,t) = DWF * \left((1 - EISF_M)\exp\left(-\left(\frac{t}{\tau_M}\right)^{\beta_M}\right) + (EISF_M - EISF_\gamma)\exp\left(-\left(\frac{t}{\tau_\gamma}\right)^{\beta_\gamma}\right) + EISF_\gamma \right). \quad (15)$$

$EISF_\gamma$, τ_γ and β_γ are the corresponding elastic incoherent structure factor, the relaxation time and the shape parameter. An example for the fit is included in Figure 12. Again Equ. 14 is used to calculate a mean relaxation time from τ_γ. The corresponding relaxation rates are included to Figure 5. The estimated relaxation rate from neutron scattering agree well with the data of the dielectric γ-relaxation.

Haverkate et al.[60] revealed the dynamics of HAT6 at picosecond time scale by quasi-elastic neutron scattering. (Some further data are also published elsewhere by the same group of authors[75,76]) The experimental data obtained by neutron scattering were compared with molecular dynamic simulations. For the simulations only twelve columns having six molecules have been considered. This model does not consider the full liquid crystalline structure in the hexagonal ordered phase of HAT6. In the quasi-elastic neutron scattering spectra two relaxation processes were observed, a slow process and a fast process which has a relaxation time which is ca. 2 orders of magnitude shorter than that of the slow process. Considering the simulation results the slow process is attributed to rotational fluctuations of the core (tilt and twist), where the movements of the core and the alkyl chains are correlated. The fast process is assigned to translational fluctuations of the core (parallel and perpendicular to the column axis), where the alkyl chains motions are only weakly correlated with the parallel motion of the core. The neutron scattering data reported by Haverkate et al.[60] are included in Figure 5. The comparison with the data measured here reveals that the process with the shorter relaxation time cannot be observed in our experiments in the selected configuration of the TOF spectrometer. Nevertheless, our data are consistent with a process at

shorter timescale because our incoherent intermediate time dependent scattering function is for the measured shortest time $S_{Inc}(q,t)<1$ (see Figure 12). The process with the longer relaxation time corresponds well to that of the methyl group rotation observed here. In the light of this discussion the interpretation of the data in ref.[60] seems to be at least questionable.

Conclusions

Discotic liquid crystals have promising potential applications in electronics, solar cells etc. For most applications an understanding of the molecular dynamics is required to tune the discotic liquid crystals for applications. Here the molecular dynamics of model discotic liquid crystal, Hexakis(hexa-alkyloxy)triphenylene (HAT6) is investigated by a combination of broadband dielectric spectroscopy, advanced calorimetry and neutron scattering. The different methods are sensitive to different probes and can so shine light on the relaxation processes from different perspectives. Besides a γ-relaxation due to localized fluctuations, one main relaxation process called α_2-relaxation was detected by dielectric spectroscopy. The relaxation rate of the α_2-relaxation is quite complex and follows neither the Arrhenius nor the Vogel-Fulcher-Tammann equation. An α_1-relaxation is observed by calorimetry. The temperature dependence of the relaxation rates of the α_1-relaxation is completely different from that of the α_2-relaxation. Therefore, it is concluded that both processes have different molecular origins. The relaxation rate of the α_1-relaxation shows a close resemblance to that of the dielectric glassy dynamics of polyethylene. For that reason, the α_1-relaxation of HAT6 is assigned to the cooperative fluctuations of the alkyl chains in the intercolumnar space, this means a glass transition. This glass transition can be considered as a one in 3-dimensional confinement. This process cannot be observed by dielectric spectroscopy because no dipole moment is involved.

The agreement of the temperature dependence of the relaxation rates of the α_2-relaxation with calorimetric data proves that this process is a glass transition. The α_2-relaxation is observed at temperatures lower than that characteristic for the α_1-process. This means that the fluctuations of the alkyl chains in the intercolumnar space are frozen. Therefore, the only motional processes in the system which might be active are small scale translational and/or small angle fluctuations of the cores. Such processes were evidenced by both molecular dynamic simulations and NMR measurements. Therefore the α_2-relaxation is assigned to small scale translational and/or small angle fluctuations of the cores. This process can be considered as a glass transition in one-dimensional fluid.

Conflicts of interest: There are no conflicts of interest to declare.

Acknowledgment: The Institut Laue-Langevin (Grenoble/France) and the Heinz Maier-Leibnitz Zentrum (Garching/Germany) are thanked for enabling the neutron scattering experiments. The German Science Foundation is acknowledged for financial support (DFG SCHO 470/21-1 and SCHO 470/25-1). We are grateful for the experimental help of MSc. Mohamed Aljaz Kolmangadi in terms of the temperature modulated DSC measurements under He atmosphere.

References:

1 P. W. Anderson *Science* 1995, **267**, 1615-1616.
2 C. A. Angel *Science* 1995, **267**, 1924-1935.
3 P. G. Debenedetti and F. H. Stillinger *Nature* 2000, **410**, 259-267.
4 J. C. Dyre *Rev. Mod. Phys.* 2006, **78** 953-972.
5 S. Kivelson and G. Tarjus *Nat. Materials* 2008, **7**, 831-833.
6 M. Ediger and P. Harrowell (2012) *J. Chem. Phys.* 2012, **137**, 080901-080915.
7 H. Vogel *Physikalische Zeitschrift* 1921, **22**, 645-646.
8 G. S. Fulcher *J. Am. Ceram. Soc.* 1925, **8**, 339-355.
9 G. Tammann and W. Hesse *Anorg. Allg. Chem.* 1926, **156**, 245-257.
10 C. A. Angell *J. Non-Cryst. Solids* 1991, **131-133**, 13-31.
11 C. A. Angell *J. Res. Natl. Inst. Stand. Technol.* 1997, **102**, 171-185
12 G. Adam and J. H. Gibbs *J. Chem. Phys.* 1965, **43**, 139-146.
13 E. J. Donth Relaxation and thermodynamics in polymers: glass transition, Akademie Verlag, Berlin, 1992.
14 L. Berthier, G. Biroli, J.-P. Bouchaud, L. Cipelletti, D. El Masri, F. Ladieu and M. Pierno *Science* 2005, **310**, 1797-1800.
15 Th. Bauer, P. Lunkenheimer and A. Loidl *Phys. Rev. Lett.* 2013, **111**, 225702-1 – 225702-5.
16 G. P. Johari and M. Goldstein *J. Chem. Phys.* 1970, **53**, 2372
17 G. P. Johari (1976) in *The Glass Transition and the Nature of the Glassy State*, eds. M. Goldstein and R. Simha *Ann. N.Y. Acad. Sci.* 1976, **279**, 117.
18 H. Suga and S. Seki *J. Non-Cryst. Solids* 1974, **16**, 171-194.
19 L. M Wang and R. Richert *J. Chem. Phys.* 2004, **121**, 11170-11176.
20 D. L. Leslie-Pelecky and N. O. Birge *Phys. Rev. Lett.* 1994, **72**, 1232-1236.
21 B. Kuchta, M. Descamps and F. Affouard *J. Chem. Phys.* 1998, **109**, 6753-6763.
22 S. Benkhof, T. Blochowicz, A. Kudlik, C. Tschirwitz and E. Rössler *Ferroelectrics* 2000, **236**, 193-207.
23 R. Brand, P. Lunkenheimer and A Loidl *J. Chem. Phys.* 2002, **116**, 10386-10401.
24 C. Krause, H. Yin, C. Cerclier, D. Morineau, A. Wurm, C. Schick, F. Emmerling and A. Schönhals *Soft Matter* 2012, **8**, 11115-11122.
25 H. Groothues, F. Kremer, P. G. Schouten and J. M. Warman Advanced Materials 1995, **7**, 283-286.
26 B. Glüsen, A. Kettner, J. Kopitzke and J. H. Wendorff *J. Non-Cryst. Solids* 1998, **241**, 113-120.
27 *Handbook of Liquid Crystals*, eds. D. Demus, J. Goodby, G. W. Gray, H. W. Spiess and V. Vill, Wiley-VCH, Weinheim, 1998.
28 K. S. Novoselov, A. K. Geim, S. V. Morozov, D. Jiang, M. I. Katsnelson, I. V. Grigorieva, S. V. Dubonos and A. A. Firsov *Nature*, 2005, **438**, 197-200.
29 S. Sergeyev, W. Pisula and Y.-H. Geerts *Chem. Soc., Rev.*, 2007, **36**, 1902-1929.
30 Wöhrle, I. Wurzbach, J. Kirres, A. Kostidou, N. Kapernaum, J. Litterscheidt, J. C. Haenle, P. Staffeld, A. Baro, F. Giesselmann, S. Laschat, *Chem. Rev.*, 2016, **116**, 1139–1241.
31 A. Yildirim, A. Bühlmeyer, S. Hayashi, J. C. Haenle, K. Sentker, C. Krause, P. Huber, S. Laschat, A. Schönhals *Phys. Chem. Chem. Phys.* 2019, **21**, 18265-18277.
32 M. M. Elmahdy, G. Floudas, M. Mondeshki, H. W. Spiess, X. Dou, K. Müllen *Phys. Rev. Let.* **2008**, 100, 107801.
33 M. M. Elmahdy, X. Dou, M. Mondeshki, G. Floudas, H. J. Butt, H. W. Spiess, K Müllen, *J. Am. Chem. Soc.* **2008**, 130, 5311–5319.
34 N. Haase, C. Grigoriadis, H. J. Butt, K. Müllen, G. Floudas, G. *J. Phys. Chem. B* **2011**, 115, 5807–5814.
35 C. Krause, R. Zorn, F. Emmerling, J. Falkenhagen, B. Frick, P. Huber and A. Schönhals *Phys. Chem. Chem. Phys.* 2014, **16**, 7324-7333.
36 J. E. K. Schawe, J. *Therm. Anal. Calorim.*, 2014, **116**, 1165−1173.
37 V. Mathot, M. Pyda, T. Pijpers, G. Vanden Poel, E. van De Kerkhof, S. van Herwaarden, F. van Herwaarden, A. Leenaers, *Thermochim. Acta*, 2011, **522**, 36–45.
38 V. Mathot, M. Pyda, T. Pijpers, G. V. Poel, E. van de Kerkhof, S. van Herwaarden, F. von Herwarden, A. Leenaers (2011) Thermochmica Acta **522**, 36-45
39 http://www.xensor.nl/pdffiles/sheets/nanogas3939.pdf.
40 H. Huth, A. A. Minakov and C. Schick, *J. Polym. Sci., Part B: Polym. Phys.*, 2006, **44**, 2996–3005.
41 Zhou D, Huth H, Gao Y, Xue G, Schick C (2008) *Macromolecules* 2008, **41**, 7662-7666
42 F. Kremer and A. Schönhals, Broadband dielectric measurement techniques in Broadband Dielectric Spectroscopy, eds. F. Kremer and A. Schönhals, Springer, 2003, pp 36-57.
43 M. Bée, Quasielastic neutron scattering. Principles and applications in solid state chemistry, biology and materials science, Adam Hilger, 1988.
[44] A. Schönhals, R. Zorn, B. Frick (2016) Inelastic fixed window scans on a nanoconfined discotic liquid crystal. Institut Laue-Langevin (ILL) doi:10.5291/ILL-DATA.6-07-20.
45 R. Zorn *Nucl. Instr. Meth. A* 2009, **603**, 439-445.
46 Heinz Maier-Leibnitz Zentrum, TOFTOF: Cold neutron time-of-flight spectrometer *Journal of large-scale research facilities* 2015, **1**, A15, DOI: http://dx.doi.org/10.17815/jlsrf-1-40.
47 Heinz Maier-Leibnitz Zentrum, SPHERES: Backscattering spectrometer *Journal of large-scale research facilities* 2015, **1**, A30. http://dx.doi.org/10.17815/jlsrf-1-38
48 J. Wuttke, A. Budwig, M. Drochner, H. Kämmerling, F.-J- Kayser, H. Kleines, V. Ossovyl, L- C. Pardo, M- Prager, D. Richter, G. J. Schneider, H. Schneider, S. Staringer *Rev. Sci. Instr.* 2012, **83**, 075109.
49 F. Rieutord, INX-Program for time-of-flight data reduction, ILL internal publication 90RI17T (1990)

50 O. G. Randl, SQW - A comprehensive user manual, ILL internal publication 96RA07T (1996)
51 R. Zorn, B. Frick, and L. Fetters, *Journal of Chemical Physics* 2002, **116**, 845-853.
52 A. Schönhals and F. Kremer Analysis of dielectric spectra in *Broadband Dielectric Spectroscopy*, eds. F. Kremer and A. Schönhals, Springer, Berlin, 2003, pp 59-98
53 Z. Yildirim, M. Wübbenhorst, E. Mendes, S. J. Picken, I. Paraschiiv, A. T. M. Marcelis, H. Zuilhof and E. J. R. Sudhölter *J. Non-Cryst. Solids* 2005, **351**, 2622-2628.
54 See the website of PerkinElmer: www.hyperdsc.com.
55 E. Donth, Glasübergang, Akademieverlag, Berlin 1981.
56 E. Donth, *J. Non. Cryst. Solids*, 1982, **53**, 325−330.
57 O. van den Berg, W. G. F. Sengers, W. F. Jager, S. J. Picken and M. Wübbenhorst, *Macromolecules*, 2004, **37**, 2460
58 Z. Yildirim, M. Wübbenhorst, E. Mendes, S. J. Picken, I. Paraschiv, A. T. M. Marcelis, H. Zuilhof, E. J. R. Sudhölter, *J. Non-Cryst. Solids* 2005, **351**, 2622–2628.
59 A. Yildirim, P. Szymoniak, K. Sentker, M. Butschies, A. Bühlmeyer, P. Huber, S. Laschat, A. Schönhals, *Phys. Chem. Chem. Phys.* 2018, **20**, 5626−5635.
60 L. A. Haverkate, M. Zbiri, M. R. Johnson, B. Deme, F. M. Mulder, G. J. Kearley, J. Phys. Chem. B, 2011, 115, 13809–13816.
61 Donth, E. The Glass Transition: Relaxation Dynamics in Liquids and Disordered Materials; Springer: Berlin Germany, 2001.
62 A. Schönhals and F. Kremer Theory of dielectric relaxation in *Broadband Dielectric Spectroscopy*, eds. F. Kremer and A. Schönhals, Springer, Berlin, 2003, pp 1-33.
63 A. Schönhals and F. Kremer Molecular dynamics in polymer model systems in *Broadband Dielectric Spectroscopy*, eds. F. Kremer and A. Schönhals, Springer, Berlin, 2003, pp 226-293
64 C. Lorthioir, A. Alegria, J. Colmenero Phys. Rev. E. 2003, **68**, 031805
65 S. Capaccioli, K. L. Ngai, N. Shinyashiki J. Chem Phys. B 2007, **111**, 8197-8209.
66 S. Cerveny, A. Alegria, J. Colmenero Phys. Rev. E 2008, **77**, 031803
67 A. Schönhals, H. Goering, C. Schick, B. Frick, M. Mayorova, R. Zorn Eur. Phys. J. Special Topics 2007, **141**, 255.
68 A. Schönhals, H. Goering, C. Schick, B. Frick, R. Zorn J. Non-Cryst. Solids 2005, **351**, 2668 – 2677.
69 C. Krause, R. Zorn, B. Frick and A. Schönhals *EPJ Web of Conferences* 2015, **83**, 02017.
70 C. Krause, R. Zorn, B. Frick and A. Schönhals *Colloid Polym. Sci.* 2014, **292**, 1949-1960.
71 J. Colmenero, A. Moreno and A. Alegria *Progress in Polymer Science* 2005, **30**, 1147-1184.
72 A. Schönhals, C. Schick, H. Huth, B. Frick, M. Mayorova and R. Zorn *J. Non-Cryst. Solids* 2007, **353**, 3853-3861.
73 M. Prager, A. Heidemann *Chem. Rev.* 1997, **97**, 2933-2966.
74 A. Schönhals, R. Zorn and B. Frick *Polymer* 2016, **195**, 393-406.
75 L. A. Haverkate, M. Zbiri, M. R. Johnson, E. Carter, A. Kotlewski, S. J. Picken, F. M. Mulder, G. J. Kearley, *J. Chem. Phys*., 2014, **140**, 014903.
76 L. Haverkate, M. Zbiri, M. R. Johnson, B. Deme, H. J. M. de Groot, F. Lefeber, A. Kotlewski, S. J. Picken, F. M. Mulder, F. G. J. Kearley *J. Phys. Chem. B* 2012, **116**, 13098−13105.